



Structure-based design of benzo[e]isoindole-1,3-dione derivatives as selective GSK-3 β inhibitors to activate Wnt/ β -catenin pathway



Hong Yue, Feng Lu, Chen Shen, Jun-Min Quan *

Key Laboratory of Structural Biology, School of Chemical Biology & Biotechnology, Peking University, Shenzhen Graduate School, Shenzhen 518055, China

ARTICLE INFO

Article history:

Received 5 April 2015

Available online 29 May 2015

Keywords:

GSK-3 β

Inhibitor

Wnt/ β -catenin pathway

Neurodegenerative diseases

CDK2

ABSTRACT

Deregulation of Wnt/ β -catenin pathway is closely related to the pathogenesis of neurodegenerative diseases such as Alzheimer's disease (AD), and glycogen synthase kinase 3 β (GSK-3 β), the central negative regulator of Wnt pathway, is regarded as an important target for these diseases. Here, we report a series of benzo[e]isoindole-1,3-dione derivatives as selective GSK-3 β inhibitors by rational-design and synthesis, which show high selectivity against GSK-3 β over Cyclin-dependent kinase 2 (CDK2), and significantly activate the cellular Wnt/ β -catenin pathway. The structure–activity relationship of these GSK-3 β inhibitors was also explored by *in silico* molecular docking.

© 2015 Elsevier Inc. All rights reserved.

1. Introduction

Wnt/ β -catenin signaling pathway plays essential roles in embryonic development and tissue homeostasis [1–5]. Deregulation of Wnt/ β -catenin pathway is closely associated with neurodegenerative diseases such as Alzheimer's disease [6–8], Parkinson disease [9,10] and Schizophrenia [11,12]. Glycogen synthase kinase 3 β (GSK-3 β) acts as the key negative regulator of Wnt/ β -catenin signaling pathway, and is therefore regarded as an important target for these diseases [13–18].

GSK-3 β is a constitutively active serine/threonine protein kinase belonging to the CMGC protein kinase family that include cyclin-dependent kinases (CDKs), mitogen-activated protein kinases (MAP kinases), glycogen synthase kinases (GSK-3) and CDK-like kinases. The structure of GSK-3 β is highly homologous to that of other CMGC members such as cyclin-dependent kinases (CDKs) [19–21]. In consistent with this homology, many GSK-3 β inhibitors are also potent inhibitors of CDKs [22–25]. Selectivity is thus considered as a major issue to develop potent GSK-3 β inhibitors as probes for biological functions of GSK-3 β and drugs for the treatment of various diseases [18,26–31].

During our development of a chemical genetic approach to analyzing biological systems by using zebrafish assay, we identified a potent GSK-3 β inhibitor (Fig. 1, compound **1**) bearing a benzo[e]isoindole-1,3-dione core structure from a public library, which inhibits the eye and forebrain formations of zebrafish embryos, resembling a typical Wnt overexpression phenotype

[32]. A series of synthetically more feasible derivatives (Fig. 1, compounds **1a** and **1b**) are also developed to inhibit GSK-3 β and activate Wnt pathway, but the selectivity of these inhibitors over CDK2 is relatively low [33], which is similar to that of compound **1**. Kinase selectivity profiling has shown that compound **1** is highly selective against GSK-3 β over other kinases except for CDK2 [32]. In this study, we optimized these inhibitors to be highly selective to GSK-3 β over CDK2 by structure-based rational design.

2. Results and discussion

2.1. Rational design of selective GSK-3 β inhibitors

The homology between the ATP sites of GSK-3 β and CDK2 is over 86%, so many GSK-3 β inhibitors also potentially inhibit CDK2. For example, compound **1b** inhibits GSK-3 β and CDK2 with a comparable potency. To improve the selectivity, we explored the regions outside the ATP site based on the crystal structures of GSK-3 β and CDK2, and searched for the potential residues that can be used to design selective GSK-3 β inhibitors. Detailed structural analysis revealed that the residues located at the helix D immediately following the hinge region are significantly different between GSK-3 β and CDK2 (Fig. 2). GSK-3 β is characterized by positively charged residues (Arg141 and Arg144) in this region, while CDK2 is characterized by negatively charged residues (Asp86 and Asp92). The difference of the electrostatic potential in this region makes it possible to design selective inhibitors against GSK-3 β but not CDK2. We used compound **1b** as the starting point, and introduced sulfonyl group to interact with the positively charged

* Corresponding author.

E-mail address: quanjm@pkusz.edu.cn (J.-M. Quan).

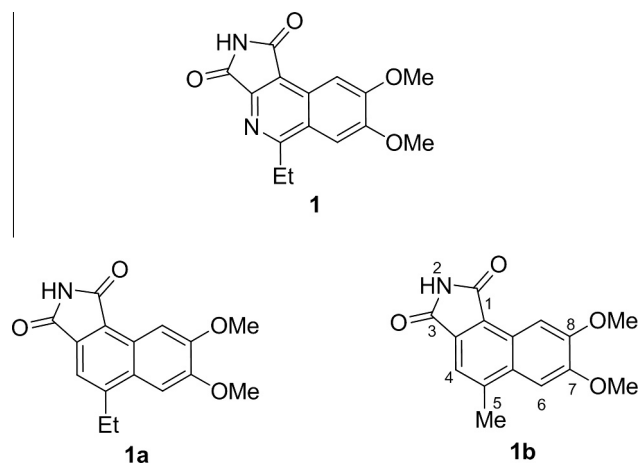


Fig. 1. Chemical structures of GSK-3 β inhibitors (**1**, **1a** and **1b**) with benzo[e]isindole-1,3-dione core structure.

residues Arg141 and Arg144 at the helix D of GSK-3 β . The sulfonyl group could be linked to the methyl group at the 5-position of the benzo[e]isindole-1,3-dione scaffold by 4-amino piperidine group with the consideration of size and solubility of the linker. Such modification of compound **1b** would improve the binding affinity with GSK-3 β by the favorable electrostatic interactions, while which might impair the binding affinity with CDK2 due to the repulsion between the partially negatively charged sulfonyl group and the negatively charged residues of CDK2.

2.2. Chemistry

The desired benzo[e]isindole-1,3-dione derivatives **8a–i** were synthesized in modest to good yields as shown in **Scheme 1**. The sulfonyl piperidine amine substrates (**5a–i**) were synthesized by the condensation of 4-Boc-aminopiperidine and sulfonyl chloride followed by removing the Boc protecting group. The precursor **6** that has been reported previously [33] served as the starting material. After bromination with NBS and AIBN, the compound **7**

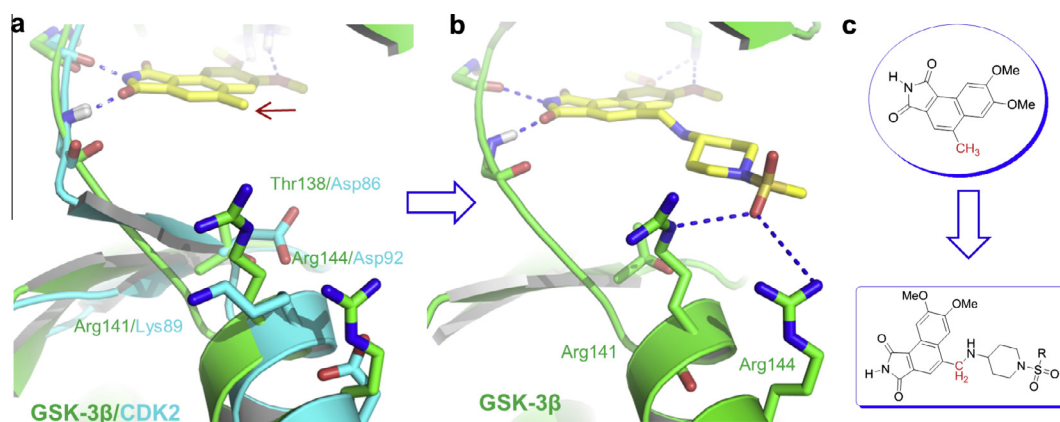
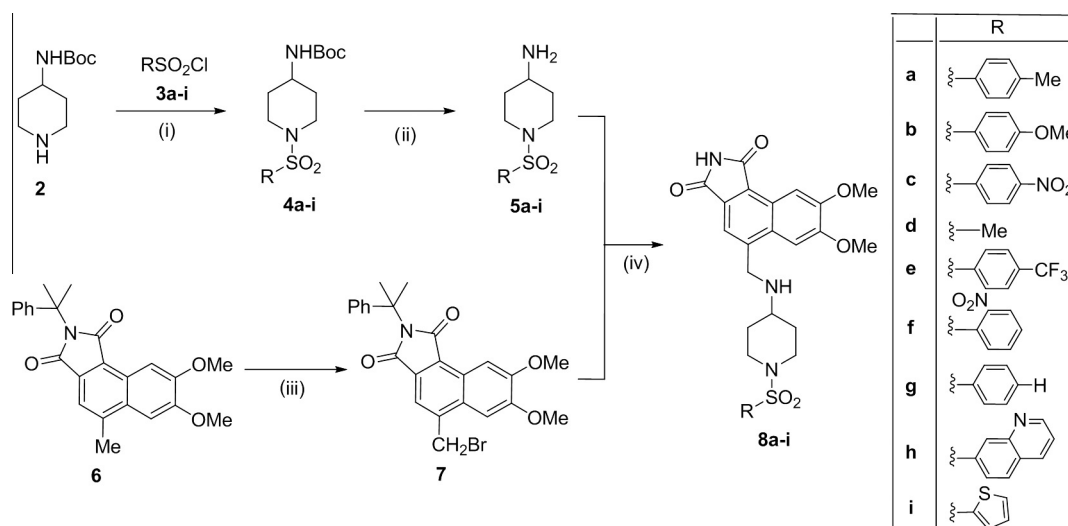


Fig. 2. Designed strategy of selective GSK-3 β inhibitors. (a) Structural comparison between GSK-3 β (green) and CDK2 (cyan), different residues at the helix D were shown in stick representation. (b) Interaction between the designed inhibitor and GSK-3 β , the hydrogen bonds were shown by blue dash lines. (c) Chemical modifications of the parent compound **1b** to selective GSK-3 β inhibitors.



Scheme 1. Synthesis of **8a–i**. (i) Boc₂O, DCM, Et₃N, stirring, rt, 4 h; (ii) TFA, stirring, rt, 10 h; (iii) NBS, AIBN, DCM, stirring, 40 °C; (iv) K₂CO₃, THF, 0 °C to room temperature, stirring overnight; and then TFA, stirring, 50 °C, 10 h.

coupled with the sulfonyl piperidine amine substrates under the classic SN2 reaction conditions (K_2CO_3 , THF, 0 °C to room temperature). The coupled product was refluxed in trifluoroacetic acid to remove the protected group of isobutyl benzene (Cumene). The final products **8a–i** were obtained, and characterized by 1H NMR, ^{13}C NMR and ESI-MS spectra.

2.3. Kinase inhibition assay

All the compounds (**8a–i**) were evaluated for their in vitro inhibitory activity against GSK-3 β and CDK2 by using Kinase Glo[®] Luminescent Kinase Assay (Promega) [34–36], and compound **1b** was also tested as reference compound (Table 1). IC_{50} values of most of these derivatives against CDK2 were much higher than 100 μM , percentage inhibitions of CDK2 were therefore measured at 100 μM for all the tested compounds. Compared with compound **1b** ($IC_{50} = 1.01 \pm 0.14 \mu M$), more than half of the compounds have improved inhibitory activity against GSK-3 β ($IC_{50} < 1 \mu M$). More strikingly, all the modified derivatives (**8a–i**) showed decreased inhibitory activity against CDK2, especially, **8d** and **8i** did not significantly inhibit CDK2 even at 100 μM . This result indicates that the different electrostatic potential in the helix D between GSK-3 β and CDK2 can be explored to design highly selective GSK-3 β inhibitors over CDK2.

To further understand the mechanism of GSK-3 β inhibited by these compounds, kinase assays were tested with the three most potent compounds **8c**, **8d** and **8i** in varied ATP concentrations. The inhibition of GSK-3 β by these three compounds was reduced with the increasing concentration of ATP, which is consistent with the direct competitive inhibition with ATP (Fig. 3).

To delineate the structure–activity relationship (SAR) of these compounds, we applied molecular docking to analyze the interactions between the inhibitors and GSK-3 β [37]. Compared with

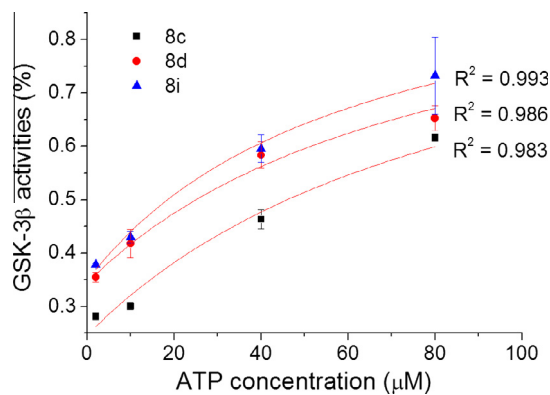


Fig. 3. Plot of relative GSK-3 β activity in the presence of **8c**, **8d**, and **8i** (1 μM) as a function of ATP concentration. The data were fitted to an equation for simple competitive inhibition: $GSK-3\beta$ activity (% of control) = $(K_{d-ATP} + [ATP]) \times 100 / (K_{d-ATP} + [ATP] + (K_{d-ATP}/K_i)[I])$, where $[I] = 1 \mu M$, I , inhibitors.

compound **1b**, the derivatives bearing the sulfonyl group including **8c–f** and **8i** have modestly improved inhibitory activity against GSK-3 β . The docking structures revealed that these compounds have favorable electrostatic interactions with the positively charged surface in the helix D of GSK-3 β by the partially negatively charged sulfonyl oxygen or the terminal functional group (Fig. 4). Compared with **8d** bearing the terminal methyl group, several derivatives (**8a**, **8b**, **8g**, and **8h**) bearing larger hydrophobic terminal functional group showed decreased inhibition against GSK-3 β , which might be explained by the unfavorable interactions between the large hydrophobic functional group of the inhibitors and the highly polar surface of GSK-3 β . In addition, all the derivatives bearing the sulfonyl group have lower inhibitory activity against CDK2

Table 1
GSK-3 β and CDK2 inhibitory activity of compounds **1b** and **8a–i**.

Entry	Products	R	IC_{50} for GSK-3 β (μM)	Inhibition for CDK2 (%) at 100 μM
1	1b	—	1.01 ± 0.14	67.4 ± 1.2
2	8a		3.73 ± 0.23	35.4 ± 9.5
3	8b		2.61 ± 0.22	8.7 ± 0.9
4	8c		0.31 ± 0.03	12.3 ± 6.3
5	8d		0.36 ± 0.06	3.4 ± 1.5
6	8e		0.53 ± 0.11	23.7 ± 3.4
7	8f		0.53 ± 0.03	16.9 ± 3.0
8	8g		1.03 ± 0.16	40.8 ± 7.5
9	8h		1.53 ± 0.35	12.3 ± 4.1
10	8i		0.54 ± 0.09	2.7 ± 1.2

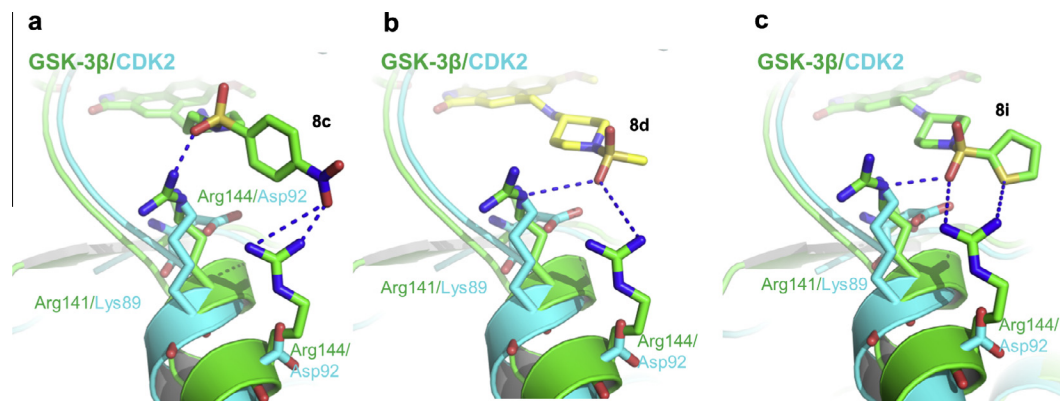


Fig. 4. Docked structures of **8c**, **8d**, and **8i** with GSK-3 β (green), CDK2 (cyan) was also shown for analysis.

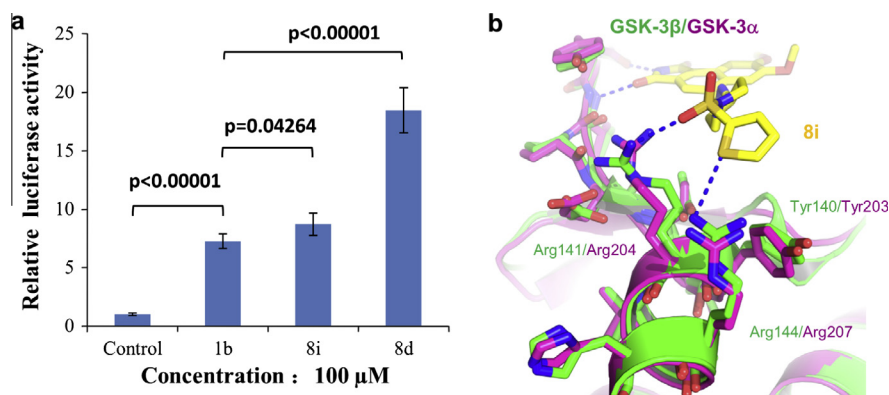


Fig. 5. (a) Wnt pathway activation by **1b**, **8d**, and **8i**. (b) Structural comparison of helix D between GSK-3 α (Magenta) and GSK-3 β (Green). The identical residues around this region are shown by stick representations.

compared to compound **1b**, which is consistent with the above-mentioned analysis that the repulsion between the partially negatively charged sulfonyl group and the negatively charged residues in the helix D of CDK2 might impair the interactions between them. We note that the docking modeling should be considered as a qualitative method rather than a quantitative method to analyze the subtle SAR for these compounds.

2.4. Wnt activation assay

To evaluate the optimization of the GSK-3 β inhibitors in the cellular level, we tested the activating activity of the most potent and selective derivatives **8d** and **8i** on Wnt/ β -catenin pathway by using Dual-Luciferase Report Assay System (Promega) [38,39], compound **1b** was also tested for comparison. **1b** activates the Wnt/ β -catenin pathway by about 4 folds at 100 μ M compared with the DMSO control. Notably, **8d** activates the Wnt/ β -catenin pathway by about 11 folds at 100 μ M, and **8i** also has significantly improved activity but to less extent compared with **8d** (Fig. 5a). This result is consistent with their *in vitro* inhibitory activity against GSK-3 β . Alternatively, these compounds might activate the Wnt/ β -catenin pathway by inhibiting GSK-3 α , a close homolog of GSK-3 β , that shares high similarity in the helix D as that of GSK-3 β (Fig. 5b) [27], and also has similar functions in the Wnt/ β -catenin pathway as that of GSK-3 β [40].

3. Conclusion

In summary, detailed structural analysis revealed a difference of electrostatic potential of the helix D outside the ATP sites between GSK-3 β and CDK2, which was explored to optimize a series of

benzo[e]isoindole-1,3-dione derivatives as selective GSK-3 β inhibitors over CDK2. These activities of the derivatives were evaluated by the *in vitro* and cellular assays, and the structure–activity relationship was analyzed by *in silico* molecular docking. The most active and selective compound **8d** inhibits GSK-3 β at submicromolar concentration ($IC_{50} = 0.34 \pm 0.14 \mu$ M), while exhibits no significant inhibition against CDK2 (3.4% inhibition at 100 μ M). Such selective GSK-3 β inhibitors can be used to explore the biological functions of GSK-3 β and also serve as lead candidates for future drug development.

4. Experimental

4.1. General

All the chemicals were purchased commercially and used without further purification, unless otherwise specified. Anhydrous dichloromethane (DCM), diisopropylamine (DIPA) and triethylamine (Et_3N) was distilled from calcium hydride (CaH_2). Dried tetrahydrofuran (THF) were distilled from sodium benzophenone. Yields refer to isolated pure products after silica gel column chromatography. Reactions were monitored by thin-layer chromatography (TLC) on silica gel plates (0.25 mm, 60F-254) using acidic anisaldehyde or basic aqueous potassium permanganate ($KMnO_4$) and UV light as visualizing method. Tsingdao silica gel (60, particle size 0.040–0.063 mm) was used for flash column chromatography. 1H NMR and ^{13}C NMR spectra were recorded on a Bruker Avance 300 (1H , 300 MHz; ^{13}C , 75.5 MHz), Bruker Avance 400 (1H , 400 MHz; ^{13}C , 100 MHz) or Bruker Avance 500 (1H , 500 MHz; ^{13}C , 125 MHz) spectrometer. The following abbreviations were used to explain the multiplicities: s = singlet,

d = doublet, t = triplet, q = quartet, m = multiplet, brs = broad. Mass spectrometric data were obtained using QSTAR Elite mass spectrometer. Melting points were measured by X-4B micromelting point detector.

4.2. General procedure for synthesis of compound **4a–i**

To a stirred solution of **2** (0.20 g, 1.00 mmol) in anhydrous DCM (5 mL) was added Et₃N (0.42 mL, 3.00 mmol) at room temperature. Then **3a–i** (3.96 mmol) was added in small portions at room temperature. The reaction was stirred for 4 h at this temperature and then quenched the reaction with saturated aqueous solution of NaHCO₃. The aqueous layer was extracted with ethyl acetate (3 × 10 mL). The combined organic layers were dried over anhydrous Na₂SO₄, filtered, and concentrated. Silica gel flash column chromatography (EtOAc/hexanes = 1:2) of the residue gave **4a–i** as the product. Dissolved **4a–i** (0.34 g, 0.97 mmol) in 25 mL TFA at room temperature, the reaction was stirred at room temperature for 10 h. Distilled the TFA under vacuum and then diluted with saturated aqueous solution of NaHCO₃. The aqueous layer was extracted with ethyl acetate (3 × 10 mL). The combined organic layers were dried over anhydrous Na₂SO₄, filtered, and concentrated. Silica gel flash column chromatography (EtOAc/hexanes = 1:1) of the residue gave **5a–i** as the product.

4.2.1. 1-tosylpiperidin-4-amine (**4a**)

4a was obtained as a white solid in 97% yield. ¹H NMR (500 MHz, CDCl₃) δ 7.55 (d, *J* = 8.1 Hz, 2H), 7.25 (d, *J* = 8.0 Hz, 2H), 4.71 (d, *J* = 7.2 Hz, 1H), 3.59 (s, 2H), 3.29 (s, 1H), 2.35 (s, 5H), 1.87 (d, *J* = 11.3 Hz, 2H), 1.53–1.37 (m, 2H), 1.32 (s, 9H); ¹³C NMR (125 MHz, CDCl₃) δ 155.05, 143.57, 133.11, 129.66, 127.58, 79.29, 47.04, 45.21, 31.63, 28.32, 21.44. HRMS (+ESI) *m/z* calcd. for C₁₇H₂₆N₂NaO₄S (M + Na)⁺ 377.1511; found 377.1506. Mp: 163–165 °C.

4.2.2. 1-(4-methoxyphenylsulfonyl) piperidin-4-amine (**4b**)

4b was obtained as a white solid in 87% yield. ¹H NMR (400 MHz, CDCl₃) δ 7.64 (d, *J* = 8.7 Hz, 2H), 6.96 (d, *J* = 8.7 Hz, 2H), 4.54 (s, 1H), 3.83 (s, 3H), 3.62 (d, *J* = 9.3 Hz, 2H), 3.38 (d, *J* = 42.1 Hz, 1H), 2.37 (t, *J* = 10.7 Hz, 2H), 1.92 (d, *J* = 9.4 Hz, 2H), 1.52–1.41 (m, 2H), 1.38 (d, *J* = 13.8 Hz, 9H); ¹³C NMR (100 MHz, CDCl₃) δ 163.02, 155.03, 129.69, 127.64, 114.25, 79.46, 55.62, 47.06, 45.22, 31.69, 28.34. HRMS (+ESI) *m/z* calcd. for C₁₇H₂₆N₂NaO₅S (M + Na)⁺ 393.1460; found 393.1454. Mp: 165–166 °C.

4.2.3. 1-(4-nitrophenylsulfonyl) piperidin-4-amine (**4c**)

4c was obtained as a pale yellow solid in 98% yield. ¹H NMR (500 MHz, CDCl₃) δ 8.43–8.34 (m, 2H), 8.01–7.91 (m, 2H), 4.42 (s, 1H), 3.75 (d, *J* = 10.4 Hz, 2H), 3.42 (s, 1H), 2.54 (s, 2H), 2.09–1.94 (m, 2H), 1.63 (s, 1H), 1.50 (dd, *J* = 11.9, 3.1 Hz, 2H), 1.41 (s, 9H); ¹³C NMR (125 MHz, CDCl₃) δ 154.91, 150.28, 128.64, 124.35, 79.79, 46.98, 45.10, 31.79, 28.32. HRMS (+ESI) *m/z* calcd. For C₁₆H₂₃N₃NaO₆S (M + Na)⁺ 408.1205; found 408.1201. Mp: 228–229 °C.

4.2.4. 1-(methylsulfonyl)piperidin-4-amine (**4d**)

4d was obtained as a colorless oil liquid in 55% yield. ¹H NMR (400 MHz, CDCl₃) δ 4.55 (d, *J* = 6.0 Hz, 1H), 3.72 (d, *J* = 11.7 Hz, 2H), 3.54 (s, 1H), 2.88–2.69 (m, 5H), 2.07–1.93 (m, 2H), 1.52–1.44 (m, 2H), 1.42 (s, 9H); ¹³C NMR (100 MHz, CDCl₃) δ 155.08, 79.68, 47.22, 45.05, 34.88, 31.98, 28.38. HRMS (+ESI) *m/z* calcd. for C₁₁H₂₂N₂NaO₄S (M + Na)⁺ 301.1198; found 301.1192. Mp: 162–163 °C.

4.2.5. 1-(4-(trifluoromethyl)phenylsulfonyl) piperidin-4-amine (**4e**)

4e was obtained as a white solid in 75% yield. ¹H NMR (500 MHz, CDCl₃) δ 7.88 (d, *J* = 8.2 Hz, 2H), 7.80 (d, *J* = 8.2 Hz, 2H), 4.45 (s, 1H), 3.71 (d, *J* = 8.7 Hz, 2H), 3.41 (s, 1H), 2.50 (t, *J* = 11.1 Hz, 2H), 1.98 (d, *J* = 11.0 Hz, 2H), 1.49 (dd, *J* = 20.6, 11.1 Hz, 2H), 1.40 (s, 9H); ¹³C NMR (125 MHz, CDCl₃) δ 154.94, 140.43, 134.67, 134.41, 128.00, 126.25, 126.22, 124.30, 122.13, 79.68, 47.03, 45.09, 31.78, 28.31. HRMS (+ESI): *m/z* calcd. for C₁₇H₂₃F₃N₂NaO₄S (M + Na)⁺ 431.1228; found 431.1221. Mp: 227–229 °C.

4.2.6. 1-(2-nitrophenylsulfonyl) piperidin-4-amine (**4f**)

4f was obtained as a white solid in 93% yield. ¹H NMR (500 MHz, CDCl₃) δ 7.89 (d, *J* = 7.3 Hz, 1H), 7.66 (dd, *J* = 13.2, 7.0 Hz, 2H), 7.55 (d, *J* = 7.3 Hz, 1H), 4.69 (d, *J* = 7.7 Hz, 1H), 3.71 (d, *J* = 12.4 Hz, 2H), 3.48 (s, 1H), 2.83 (t, *J* = 11.7 Hz, 2H), 1.93 (d, *J* = 12.0 Hz, 2H), 1.50–1.40 (m, 2H), 1.37 (s, 9H); ¹³C NMR (125 MHz, CDCl₃) δ 155.07, 148.24, 133.79, 131.67, 130.72, 124.09, 79.45, 47.05, 44.90, 31.90, 28.34. HRMS (+ESI): *m/z* calcd. for C₁₆H₂₃N₃NaO₆S (M + Na)⁺ 408.1205; found 408.1200. Mp: 225–226 °C.

4.2.7. 1-(phenylsulfonyl) piperidin-4-amine (**4g**)

4g was obtained as a white solid in 95% yield. ¹H NMR (400 MHz, D-DMSO) δ 7.69 (d, *J* = 7.6 Hz, 2H), 7.54 (t, *J* = 7.2 Hz, 1H), 7.48 (t, *J* = 7.4 Hz, 2H), 4.65 (d, *J* = 6.4 Hz, 1H), 3.63 (d, *J* = 8.3 Hz, 2H), 3.31 (s, 1H), 2.37 (t, *J* = 10.0 Hz, 2H), 1.89 (d, *J* = 11.7 Hz, 2H), 1.53–1.38 (m, 2H), 1.34 (s, 9H); ¹³C NMR (125 MHz, CDCl₃) δ 155.04, 136.23, 132.79, 129.05, 127.51, 79.35, 77.43, 77.17, 76.92, 47.06, 45.20, 31.65, 28.33. HRMS (+ESI): *m/z* calcd. for C₁₆H₂₄N₂NaO₄S (M + Na)⁺ 363.1354; found 363.1350. Mp: 217–218 °C.

4.2.8. 1-(quinolin-8-ylsulfonyl) piperidin-4-amine (**4h**)

4h was obtained as a white solid in 80% yield. ¹H NMR (500 MHz, CDCl₃) δ 9.08–8.95 (m, 1H), 8.51–8.37 (m, 1H), 8.22 (dd, *J* = 8.3, 1.4 Hz, 1H), 8.01 (d, *J* = 8.1 Hz, 1H), 7.59 (t, *J* = 7.8 Hz, 1H), 7.51 (dd, *J* = 8.3, 4.2 Hz, 1H), 4.48 (s, 1H), 4.01 (d, *J* = 12.1 Hz, 2H), 3.45 (s, 1H), 2.93 (d, *J* = 11.8 Hz, 2H), 1.94 (d, *J* = 10.6 Hz, 2H), 1.82 (s, 1H), 1.44 (dd, *J* = 11.9, 3.6 Hz, 2H), 1.39 (s, 9H); ¹³C NMR (125 MHz, CDCl₃) δ 155.07, 151.09, 144.21, 137.30, 136.40, 133.35, 132.90, 129.02, 125.49, 122.01, 79.47, 47.62, 45.35, 32.63, 28.37. HRMS (+ESI): *m/z* calcd. for C₁₉H₂₆N₃O₄S (M + H)⁺ 392.1644; found 392.1639. Mp: 210–212 °C.

4.2.9. 1-(thiophen-2-ylsulfonyl) piperidin-4-amine (**4i**)

4i was obtained as a white solid in 99% yield. ¹H NMR (500 MHz, CDCl₃) δ 7.57 (dd, *J* = 5.0, 1.2 Hz, 1H), 7.46 (dd, *J* = 3.7, 1.3 Hz, 1H), 7.08 (dd, *J* = 5.0, 3.8 Hz, 1H), 4.68 (d, *J* = 7.8 Hz, 1H), 3.62 (d, *J* = 10.1 Hz, 2H), 3.34 (s, 1H), 2.45 (t, *J* = 11.0 Hz, 2H), 1.92 (d, *J* = 10.6 Hz, 2H), 1.55–1.39 (m, 2H), 1.34 (s, 9H); ¹³C NMR (125 MHz, CDCl₃) δ 155.06, 136.56, 132.30, 132.08, 127.65, 79.40, 47.01, 45.27, 31.51, 28.34. HRMS (+ESI): *m/z* calcd. for C₁₄H₂₂N₂NaO₄S₂ (M + Na)⁺ 369.0919; found 369.0912. Mp: 142–143 °C.

4.3. General procedure for synthesis of compound **8a–i**

To a stirred suspension of **6** (0.36 g, 0.93 mmol) and NBS (0.17 g, 0.99 mmol) in anhydrous DCM (5 mL) was added AIBN (0.06 g, 0.36 mmol) in one portion under N₂ atmosphere at room temperature. The reaction was stirred at 40 °C. TLC analysis showed consumption of **6**. The reaction was filtered and concentrated. Silica gel flash column chromatography (EtOAc/hexanes 1:25) of the residue gave a white solid **7** (0.37 g, 0.81 mmol, 87%) as the product. To a stirred solution of **5a** (0.21 mmol) in anhydrous THF

(1 mL) was added anhydrous K_2CO_3 (56 mg, 0.40 mmol) at 0 °C. The resulting mixture was stirred at this temperature for 30 min. To this mixture was added **7** (50 mg, 0.11 mmol) at 0 °C. The resulting mixture was stirred at room temperature overnight. The reaction was quenched with saturated aqueous solution of $NaHCO_3$. The aqueous layer was extracted with ethyl acetate (3×10 mL). The combined organic layers were dried over anhydrous Na_2SO_4 , filtered, and concentrated. The crude product was dissolved in 10 mL TFA. The resulting mixture was stirred at 50 °C for 10 h. Distilled the TFA under vacuum and then diluted with saturated aqueous solution of $NaHCO_3$. The aqueous layer was extracted with ethyl acetate (3×10 mL). The combined organic layers were dried over anhydrous Na_2SO_4 , filtered, and concentrated. Silica gel flash column chromatography (EtOAc/hexanes 1:2) of the residue gave a yellow solid **8a–i** as the product.

4.3.1. 7,8-dimethoxy-5-((1-tosylpiperidin-4-ylamino)methyl)-1H-benzo[e]isoindole-1,3(2H)-dione (**8a**)

8a was obtained as a pale yellow solid in 34% two-steps yield (iv). 1H NMR (500 MHz, D-DMSO) δ 11.01 (s, 1H), 8.01 (s, 1H), 7.59 (d, $J = 8.6$ Hz, 3H), 7.41 (d, $J = 8.6$ Hz, 3H), 4.04 (d, $J = 27.8$ Hz, 2H), 3.89 (s, 3H), 3.87 (s, 3H), 3.41 (d, $J = 11.1$ Hz, 2H), 2.44–2.48 (m, 3H), 2.38 (s, 3H), 1.98–1.89 (m, 2H), 1.48–1.37 (m, 2H); ^{13}C NMR (125 MHz, D-DMSO) δ 171.56, 170.40, 152.08, 151.17, 143.85, 133.20, 131.40, 130.23, 129.58, 127.88, 124.85, 124.37, 116.48, 104.31, 102.76, 55.97, 55.94, 53.32, 48.45, 44.91, 31.43, 21.44. HRMS (+ESI): m/z calcd. for $C_{27}H_{30}N_3O_6S$ (M + H) $^+$ 524.1855; found 524.1846. Mp: 208–209 °C.

4.3.2. 7,8-dimethoxy-5-((1-(4-methoxyphenylsulfonyl)piperidin-4-ylamino)methyl)-1H-benzo[e]isoindole-1,3(2H)-dione (**8b**)

8b was obtained as a pale yellow solid in 35% two-steps yield (iv). 1H NMR (400 MHz, D-DMSO) δ 11.28 (s, 1H), 8.16 (s, 1H), 7.84 (s, 1H), 7.74–7.62 (m, 2H), 7.42 (s, 1H), 7.26–7.09 (m, 2H), 4.70 (s, 2H), 3.99 (s, 3H), 3.93 (s, 3H), 3.84 (s, 3H), 3.73 (d, $J = 11.4$ Hz, 2H), 2.48 (s, 1H), 2.25–2.33 (m, 4H), 1.73–1.71 (m, 2H); ^{13}C NMR (100 MHz, D-DMSO) δ 171.24, 169.87, 163.30, 152.62, 152.05, 134.35, 131.42, 130.17, 129.21, 127.30, 126.63, 124.57, 119.13, 115.07, 104.33, 103.01, 67.72, 67.66, 56.39, 56.21, 56.18, 54.89, 45.21, 44.95, 27.92. HRMS (+ESI): m/z calcd. for $C_{27}H_{30}N_3O_7S$ (M + H) $^+$ 540.1804; found 540.1802. Mp: 209–210 °C.

4.3.3. 7,8-dimethoxy-5-((1-(4-nitrophenylsulfonyl)piperidin-4-ylamino)methyl)-1H-benzo[e]isoindole-1,3(2H)-dione (**8c**)

8c was obtained as a pale yellow solid in 42% two-steps yield (iv). 1H NMR (400 MHz, D-DMSO) δ 11.04 (s, 1H), 8.40 (d, $J = 8.6$ Hz, 2H), 8.12–7.93 (m, 3H), 7.61 (s, 1H), 7.41 (s, 1H), 4.10 (s, 2H), 3.88 (s, 3H), 3.87 (s, 3H), 3.47 (d, $J = 11.6$ Hz, 2H), 2.60 (t, $J = 9.7$ Hz, 3H), 1.92 (t, $J = 13.4$ Hz, 2H), 1.46–1.39 (m, 2H); ^{13}C NMR (100 MHz, D-DMSO) δ 171.56, 170.40, 152.08, 151.15, 150.41, 141.90, 131.36, 129.55, 129.39, 125.10, 124.86, 124.36, 116.47, 104.29, 102.72, 55.99, 55.94, 52.97, 48.26, 46.16, 44.77, 31.27. HRMS (+ESI): m/z calcd. for $C_{26}H_{27}N_4O_8S$ (M + H) $^+$ 555.1550; found 555.1563. Mp: 221–222 °C.

4.3.4. 7,8-dimethoxy-5-((1-(methylsulfonyl)piperidin-4-ylamino)methyl)-1H-benzo[e]isoindole-1,3(2H)-dione (**8d**)

8d was obtained as a pale yellow solid in 90% two-steps yield (iv). 1H NMR (300 MHz, D-DMSO) δ 11.09 (s, 1H), 8.10 (s, 1H), 7.74 (s, 1H), 7.53 (s, 1H), 4.21 (s, 2H), 3.95 (s, 3H), 3.55–3.42 (m, 2H), 2.85–2.75 (m, 5H), 1.98 (d, $J = 7.0$ Hz, 2H), 1.48 (d, $J = 11.5$ Hz, 2H); ^{13}C NMR (75 MHz, D-DMSO) δ 171.64, 170.49, 152.16, 151.26, 131.47, 130.11, 129.65, 124.90, 124.42, 116.52, 104.43, 102.78, 56.08, 55.99, 53.66, 48.21, 44.46, 35.57,

31.70. HRMS (+ESI): m/z calcd. for $C_{21}H_{26}N_3O_6S$ (M + H) $^+$ 448.1542; found 448.1537. Mp: 206–207 °C.

4.3.5. 7,8-dimethoxy-5-((1-(4-(trifluoromethyl)phenylsulfonyl)piperidin-4-ylamino)methyl)-1H-benzo[e]isoindole-1,3(2H)-dione (**8e**)

8e was obtained as a pale yellow solid in 26% two-steps yield (iv). 1H NMR (300 MHz, D-DMSO) δ 11.06 (s, 1H), 8.07 (s, 1H), 8.00 (d, $J = 8.5$ Hz, 2H), 7.94 (d, $J = 8.4$ Hz, 2H), 7.65 (s, 1H), 7.45 (s, 1H), 4.12 (s, 2H), 3.89 (d, $J = 4.1$ Hz, 6H), 3.47 (d, $J = 7.8$ Hz, 2H), 2.52–2.54 (m, 3H), 2.00–1.92 (m, 2H), 1.44–1.41 (m, 2H); ^{13}C NMR (75 MHz, D-DMSO) δ 171.60, 170.43, 152.11, 151.18, 140.20, 133.32, 132.89, 131.42, 130.10, 129.61, 128.82, 127.07, 127.01, 125.73, 124.88, 124.39, 122.11, 116.53, 104.36, 102.74, 55.99, 55.96, 53.03, 48.32, 44.88, 31.40, 29.49. HRMS (+ESI): m/z calcd. for $C_{27}H_{27}F_3N_3O_6S$ (M + H) $^+$ 578.1573; found 578.1558. Mp: 219–220 °C.

4.3.6. 7,8-dimethoxy-5-((1-(2-nitrophenylsulfonyl)piperidin-4-ylamino)methyl)-1H-benzo[e]isoindole-1,3(2H)-dione (**8f**)

8f was obtained as a pale yellow solid in 78% two-steps yield (iv). 1H NMR (400 MHz, D-DMSO) δ 11.10 (s, 1H), 8.11 (s, 1H), 8.98–7.95 (m, 2H), 7.89–7.83 (m, 2H), 7.73 (s, 1H), 7.51 (s, 1H), 4.22 (s, 2H), 3.95 (s, 6H), 3.59 (s, 2H), 2.95–2.85 (m, 2H), 2.52 (s, 1H), 2.04–1.96 (m, 2H), 1.47–1.45 (m, 2H); ^{13}C NMR (100 MHz, D-DMSO) δ 171.28, 169.89, 152.62, 152.03, 148.22, 135.39, 132.90, 131.44, 130.86, 130.10, 129.21, 126.64, 124.71, 124.57, 119.18, 116.15, 104.38, 102.97, 56.37, 56.18, 54.77, 45.16, 44.57, 28.17. HRMS (+ESI): m/z calcd. for $C_{26}H_{27}N_4O_8S$ (M + H) $^+$ 555.1550; found 555.1442. Mp: 218–220 °C.

4.3.7. 7,8-dimethoxy-5-((1-(phenylsulfonyl)piperidin-4-ylamino)methyl)-1H-benzo[e]isoindole-1,3(2H)-dione (**8g**)

8g was obtained as a pale yellow solid in 84% two-steps yield (iv). 1H NMR (400 MHz, D-DMSO) δ 11.00 (s, 1H), 7.94 (s, 1H), 7.70 (dd, $J = 13.6, 7.2$ Hz, 3H), 7.62 (t, $J = 7.4$ Hz, 2H), 7.56 (s, 1H), 7.33 (s, 1H), 4.04 (s, 2H), 3.85 (d, $J = 6.2$ Hz, 6H), 3.45 (d, $J = 11.7$ Hz, 2H), 2.54–2.43 (m, 3H), 1.94 (dd, $J = 10.8, 6.5$ Hz, 2H), 1.45–1.38 (m, 2H); ^{13}C NMR (100 MHz, D-DMSO) δ 171.53, 170.38, 151.97, 151.08, 143.24, 136.11, 133.52, 131.29, 129.81, 129.48, 127.82, 124.77, 124.27, 104.15, 102.66, 55.93, 55.88, 53.38, 48.42, 44.96, 31.40. HRMS (+ESI): m/z calcd. for $C_{26}H_{28}N_3O_6S$ (M + H) $^+$ 510.1699; found 510.1697. Mp: 235–236 °C.

4.3.8. 7,8-dimethoxy-5-((1-(quinolin-8-ylsulfonyl)piperidin-4-ylamino)methyl)-1H-benzo[e]isoindole-1,3(2H)-dione (**8h**)

8h was obtained as a pale yellow solid in 75% two-steps yield (iv). 1H NMR (400 MHz, D-DMSO) δ 11.03 (s, 1H), 9.03 (dd, $J = 4.1, 1.5$ Hz, 1H), 8.71–8.45 (m, 1H), 8.34 (d, $J = 6.5$ Hz, 1H), 8.27 (d, $J = 8.1$ Hz, 1H), 8.04 (d, $J = 11.4$ Hz, 1H), 7.73 (t, $J = 7.8$ Hz, 1H), 7.69–7.61 (m, 1H), 7.44 (s, 1H), 4.10 (d, $J = 10.5$ Hz, 2H), 3.89 (s, 3H), 3.85 (s, 3H), 3.83–3.71 (m, 2H), 2.90 (t, $J = 10.6$ Hz, 2H), 2.58 (s, 1H), 1.96 (dd, $J = 18.9, 12.8$ Hz, 2H), 1.40–1.30 (m, 2H); ^{13}C NMR (100 MHz, D-DMSO) δ 171.59, 170.43, 152.11, 151.73, 151.17, 143.83, 137.25, 136.93, 134.31, 132.82, 131.43, 129.62, 129.20, 126.19, 124.85, 124.72, 124.38, 122.87, 116.49, 104.40, 102.77, 55.96, 53.94, 48.39, 45.03, 32.35. HRMS (+ESI): m/z calcd. for $C_{29}H_{29}N_4O_6S$ (M + H) $^+$ 561.1808; found 561.1804. Mp: 217–218 °C.

4.3.9. 7,8-dimethoxy-5-((1-(thiophen-2-ylsulfonyl)piperidin-4-ylamino)methyl)-1H-benzo[e]isoindole-1,3(2H)-dione (**8i**)

8i was obtained as a pale yellow solid in 35% two-steps yield (iv). 1H NMR (400 MHz, D-DMSO) δ 11.29 (s, 1H), 9.32 (s, 2H), 8.17 (s, 1H), 8.07 (d, $J = 4.9$ Hz, 1H), 7.86 (s, 1H), 7.67 (d, $J = 2.7$ Hz, 1H), 7.43 (s, 1H), 7.30 (dd, $J = 4.7, 4.0$ Hz, 1H), 4.73 (s,

2H), 4.04 (s, 3H), 3.94 (s, 3H), 3.77 (d, $J = 11.8$ Hz, 2H), 2.48–2.42 (m, 3H), 2.32 (d, $J = 11.0$ Hz, 2H), 1.80–1.72 (m, 2H); ^{13}C NMR (100 MHz, D-DMSO) δ 171.25, 169.88, 152.64, 152.08, 135.60, 134.49, 133.63, 131.38, 129.21, 128.87, 126.68, 124.58, 119.14, 104.31, 103.01, 67.73, 67.65, 56.43, 56.20, 54.78, 45.21, 45.03, 27.78, 20.44. HRMS (+ESI): m/z calcd. for $\text{C}_{24}\text{H}_{26}\text{N}_3\text{O}_6\text{S}_2$ ($\text{M} + \text{H}$) $^+$ 516.1263; found 516.1258. Mp: 201–202 °C.

4.4. Kinase inhibition assays

The inhibitory activity of the tested compounds against GSK-3 β and CDK2 was measured by using Kinase-Glo luminescent kinase assay (Promega). Briefly, recombinant human GSK3 β (1 μM , 10 μl) was mixed with 10 μl of GSK-3 β substrate (YRRAAVPPSPSLSRHSSPHQpSEDEEE, 100 μM), 19 μl of 2.5 \times kinase buffer (50 mM Tris-HCl, pH 7.4, 25 mM MgCl₂), 10 μl of 10 μM ATP, 1 μl of the indicated amount of chemicals in DMSO to a final volume of 50 μl . Control reaction without kinase was set up. The mixtures were incubated at 30 °C for 40 min. The enzymatic reaction was stopped with 50 μl of Kinase-Glo reagent. Glow-type luminescence was recorded after 10 min using a TECAN infinite F200 multimode reader. On the other hand, CDK2 (1 μM , 10 μl) was mixed with 10 μl of CDK2 substrate (PKTPKKAKKL, 100 μM), 19 μl of 2.5 \times kinase buffer (50 mM Tris-HCl, pH 7.4, 25 mM MgCl₂), 10 μl of 10 μM ATP, 1 μl of the indicated amount of chemicals in DMSO to a final volume of 50 μl . Control reaction without kinase was set up. The following steps were the same as the detection of GSK-3 inhibitory activity.

4.5. β -catenin–TCF reporter gene assay

L cells on 96 well plates were transfected with 200 ng TOPflash reporter plasmid and 100 ng internal control vectors pRL-SV40 using Lipofectamine TM2000 (Life, Cat. No. 11668019) and Opti-MEM (Life, Cat. No. 31985-062) according to the manufacturer's instructions. 24 h after transfection the tested compounds were added to cells at 100 μM concentration for 24 h. Control cells were DMSO vehicle treated. Then cell extracts were prepared and examined sequentially for firefly and Renilla luciferase activities using the Dual-Luciferase Reporter assay system (Promega, Madison, WI). Firefly luciferase readings were normalized against Renilla luciferase.

4.6. Molecular docking

Protein coordinates for docking were obtained from the crystal structure of GSK-3 β in complex with indirubin (PDB entry 1UV5) [41] and CDK2 in complex with indirubin (PDB entry 1E9H) [42]. The indirubin binding sites were used to dock compounds **1b** and **8a–i**. Waters and indirubin were removed from the PDB file, and the polar hydrogen atoms were added to the amino acid residues before the docking study. Docking was performed using AutoDock, version 4.0 [37]. All illustrated structures were made using PyMOL (DeLano Scientific, Palo Alto, CA) [43].

Acknowledgments

This work was supported by funds from the Ministry of Science and Technology 2012CB722602 (to J.M.Q.); the NSFC21290183 and NSFC81373326 (to J.M.Q.); Shenzhen government JCYJ20130331144947526, GJHS20120628101219329 and GJHZ20120614144733420 (to J.M.Q.).

References

- [1] R.T. Moon, A.D. Kohn, G.V. De Ferrari, A. Kaykas, *Nat. Rev. Genet.* 5 (2004) 691–701.
- [2] H. Clevers, *Cell* 127 (2006) 469–480.
- [3] B.T. MacDonald, K. Tamai, X. He, *Dev. Cell* 17 (2009) 9–26.
- [4] A. Kikuchi, H. Yamamoto, A. Sato, *Trends Cell Biol.* 19 (2009) 119–129.
- [5] H. Clevers, R. Nusse, *Cell* 149 (2012) 1192–1205.
- [6] G.V. De Ferrari, N.C. Inestrosa, *Brain Res. Rev.* 33 (2000) 1–12.
- [7] N.C. Inestrosa, L. Varela-Nallar, *J. Mol. Cell Biol.* 6 (2014) 64–74.
- [8] W. Wan, S. Xia, B. Kalionis, L. Liu, Y. Li, *BioMed. Res. Int.* 2014 (2014) 301575.
- [9] D.C. Berwick, K. Harvey, *Biochem. Soc. Trans.* 40 (2012) 1123–1128.
- [10] B. Marchetti, F. L'Episcopo, M.C. Morale, C. Tirolo, N. Testa, S. Caniglia, M.F. Serapide, S. Pluchino, *Eur. J. Neurosci.* 37 (10) (2013) 1550–1563.
- [11] D. Cotter, R. Kerwin, S. Al-Sarraj, J.P. Brion, A. Chadwick, S. Lovestone, B. Anderton, I. Everall, *Neuroreport* 9 (7) (1998) 1379–1383.
- [12] N.C. Inestrosa, C. Montecinos-Oliva, M. Fuenzalida, *J. Neuroimmune Pharmacol.* 7 (2012) 788–807.
- [13] K.K. Singh, *Clin. Genet.* 83 (6) (2013) 511–517.
- [14] X. Zeng, K. Tamai, B. Doble, S. Li, H. Huang, R. Habas, H. Okamura, J. Woodgett, X. He, *Nature* 438 (2005) 873–877.
- [15] R. Luna-Medina, M. Cortes-Canteli, S. Sanchez-Galiano, J.A. Morales-Garcia, A. Martinez, A. Santos, A. Perez-Castillo, *J. Neurosci.* 27 (2007) 5766–5776.
- [16] G. Wu, H. Huang, J.G. Abreu, X. He, *PLoS One* 4 (2009) e4926.
- [17] D. Wu, W. Pan, *Trends Biochem. Sci.* 35 (2010) 161–168.
- [18] H. Eldar-Finkelman, A. Martinez, *Front. Mol. Neurosci.* 4 (2011) 32.
- [19] M. Welcker, J. Singer, K.R. Loeb, J. Grim, A. Bloecher, M. Gurien-West, B.E. Clurman, J.M. Roberts, *Mol. Cell* 12 (2003) 381–392.
- [20] A. Vulpatti, P. Crivori, A. Cameron, J. Bertrand, M.G. Brasca, R.D. Alessio, P. Pevarello, *J. Chem. Inf. Model* 45 (5) (2005) 1282–1290.
- [21] I. Buch, D. Fishelovitch, N. London, B. Raveh, H.J. Wolfson, *R. Nussinov, Biochemistry* 49 (2010) 10890–10901.
- [22] P.M. Fischer, *Chem. Biol.* 10 (12) (2003) 1144–1146.
- [23] Y. Mettey, M. Gompel, V. Thomas, M. Garnier, M. Leost, I. Ceballos-Picot, M. Noble, J. Endicott, J.M. Vierfond, L. Meijer, *J. Med. Chem.* 46 (2003) 222–236.
- [24] T.J. Soos, L. Meijer, P.J. Nelson, *Drug News Perspect.* 19 (6) (2006) 325–328.
- [25] E. Damiens, B. Baratte, D. Marie, G. Eisenbrand, L. Meijer, *Oncogene* 20 (29) (2001) 3786–3797.
- [26] T. Kramer, B. Schmidt, F. Lo, *Int. J. Alzheimers Dis.* 2012 (2012) 381029.
- [27] L. Meijer, M. Flajolet, P. Greengard, *Trends Pharmacol. Sci.* 25 (9) (2004) 471–480.
- [28] D. Lesuisse, G. Dutruc-Rosset, G. Tiraboschi, M.K. Dreyer, S. Maignan, A. Chevalier, F. Halley, P. Bertrand, M.C. Burgevin, D. Quarteronet, T. Rooney, *Bioorg. Med. Chem. Lett.* 20 (2010) 1985–1989.
- [29] L. Avrahami, A. Licht-Murava, M. Eisenstein, H. Eldar-Finkelman, *Biochim. Biophys. Acta* 1834 (2013) 1410–1414.
- [30] B. Georgievska, J. Sandin, J. Doherty, A. Mörtberg, J. Neelissen, A. Andersson, S. Gruber, Y. Nilsson, P. Schött, P. Arvidsson, S. Hellberg, G. Osswald, S. Berg, J. Fälting, R.V. Bhat, *J. Neurochem.* 125 (3) (2013) 446–456.
- [31] D.S. Patel, P.V. Bharatam, *Eur. J. Med. Chem.* 43 (5) (2008) 949–957.
- [32] H. Zhong, H. Zou, M.V. Semenov, D. Moshinsky, X. He, H. Huang, S. Li, J. Quan, Z. Yang, S. Lin, *Mol. Biosyst.* 5 (2009) 1356–1360.
- [33] H. Zou, L. Zhou, Y. Li, H. Zhong, Z. Pan, Z. Yang, J. Quan, *J. Med. Chem.* 53 (2010) 994–1003.
- [34] M.I. Rafique, R.B. Jeffrey, *MethodsX* 1 (2014) 96–101.
- [35] J.A. Morales-García, C. Susín, S. Alonso-Gil, D.I. Pérez, V. Palomo, C. Pérez, S. Conde, A. Santos, C. Gil, A. Martínez, A. Pérez-Castillo, *Chem. Neurosci.* 4 (2013) 350–360.
- [36] A. Baki, A. Bielik, L. Molnár, G. Szendrei, G.M. Keserü, *Assay Drug Dev. Technol.* 5 (2007) 75–83.
- [37] G.M. Morris, D.S. Goodsell, R.S. Halliday, R. Huey, W.E. Hart, R.K. Belew, A.J. Olson, *J. Comput. Chem.* 19 (1998) 1639–1662.
- [38] L. Rinnab, S.V. Schütz, J. Diesch, E. Schmid, R. Küfer, R.E. Hautmann, K.D. Spindler, M.V. Cronauer, *Neoplasia* 10 (6) (2008) 624–634.
- [39] M.P. Coghlan, A.A. Culbert, D.A. Cross, S.L. Corcoran, J.W. Yates, N.J. Pearce, O.L. Rausch, G.J. Murphy, P.S. Carter, C.L. Roxbee, D. Mills, M.J. Brown, D. Haigh, R.W. Ward, D.G. Smith, K.J. Murray, A.D. Reith, J.C. Holder, *Chem. Biol.* 7 (2000) 793–803.
- [40] B.W. Doble, S. Patel, G.A. Wood, L.K. Kockeritz, J.R. Woodgett, *Dev. Cell* 12 (2007) 957–971.
- [41] L. Meijer, A.L. Skaltsounis, P. Magiatis, P. Polychronopoulos, M. Knockaert, M. Leost, X.P. Ryan, C.A. Vonica, A. Brivanlou, R. Dajani, C. Crovace, C. Tarricone, A. Musacchio, S.M. Roe, L. Pearl, P. Greengard, *Chem. Biol.* 10 (2003) 1255–1266.
- [42] T.G. Davies, P. Tunnah, L. Meijer, D. Marko, G. Eisenbrand, J.A. Endicott, M.E. Noble, *Structure* 9 (2001) 389–397.
- [43] W.L. DeLano, *The PyMOL Molecular Graphics System*, DeLano Scientific, Palo Alto, CA, USA, 2002.